Journal of Hydrology 470–471 (2012) 172–183

Contents lists available at SciVerse ScienceDirect

Journal of Hydrology

journal homepage: www.elsevier.com/locate/jhydrol

Improved predictions of saturated and unsaturated zone drawdowns in a heterogeneous unconfined aquifer via transient hydraulic tomography: Laboratory sandbox experiments

Steven J. Berg, Walter A. Illman *

Department of Earth & Environmental Sciences, University of Waterloo, Waterloo, Ontario, Canada

ARTICLE INFO

Article history:
Received 12 May 2012
Received in revised form 9 August 2012
Accepted 22 August 2012
Available online 30 August 2012
This manuscript was handled by Peter K. Kitanidis, Editor-in-Chief, with the assistance of Christophe Darnault, Associate Editor

Keywords:
Unconfined aquifer
Unsaturated zone
Subsurface heterogeneity
Hydraulic tomography
Model calibration
Model validation

SUMMARY

Interpretation of pumping tests in unconfined aquifers has largely been based on analytical solutions that disregard aquifer heterogeneity. In this study, we investigate whether the prediction of drawdown responses in a heterogeneous unconfined aquifer and the unsaturated zone above it with a variably saturated groundwater flow model can be improved by including information on hydraulic conductivity (K) and specific storage (S_s) from transient hydraulic tomography (THT). We also investigate whether these predictions are affected by the use of unsaturated flow parameters estimated through laboratory hanging column experiments or calibration of in situ drainage curves. To investigate these issues, we designed and conducted laboratory sandbox experiments to characterize the saturated and unsaturated properties of a heterogeneous unconfined aquifer. Specifically, we conducted pumping tests under fully saturated conditions and interpreted the drawdown responses by treating the medium to be either homogeneous or heterogeneous. We then conducted another pumping test and allowed the water table to drop, similar to a pumping test in an unconfined aquifer. Simulations conducted using a variably saturated flow model revealed: (1) homogeneous parameters in the saturated and unsaturated zones have a difficult time predicting the responses of the heterogeneous unconfined aquifer; (2) heterogeneous saturated hydraulic parameter distributions obtained via THT yielded significantly improved drawdown predictions in the saturated zone of the unconfined aquifer; and (3) considering heterogeneity of unsaturated zone parameters produced a minor improvement in predictions in the unsaturated zone, but not the saturated zone. These results seem to support the finding by Mao et al. (2011) that spatial variability in the unsaturated zone plays a minor role in the formation of the S-shape drawdown-time curve observed during pumping in an unconfined aquifer.

1. Introduction

In recent decades, the topic of flow to wells during pumping in unconfined aquifers has become an issue of great interest and great debate. The need to better understand and interpret the observations from these tests has led to the development of various analytical solutions (e.g., Boulton, 1954, 1963; Dagan, 1967; Kroszynski and Dagan, 1975; Streltsova, 1973; Neuman, 1972, 1974; Moench, 1997; Mathias and Butler, 2006). Mishra and Neuman (2010) provided a comprehensive review of these solutions and offered their perspectives on the advancement of the theoretical development of unconfined aquifer analysis. Mishra and Neuman (2010) also presented an approximate analytical solution for flow to a partially penetrating well in a compressible unconfined aquifer that infers saturated and unsaturated hydraulic properties from drawdowns recorded in the saturated and/or unsaturated zone. More recently, Mishra and Neuman (2011) extended the solution of Mishra and Neuman (2010) to consider a finite diameter pumping well with storage and the effects of delayed piezometer response. Mishra and Neuman's (2010, 2011) solutions are an extension of the solution developed by Tartakovsky and Neuman (2007) and adds: (i) a more flexible representation of unsaturated constitutive properties; and (ii) a finite thickness for the unsaturated zone. Mishra and Neuman (2010) used their type curve approach in conjunction with the Model-Independent Parameter Estimation and Uncertainty Analysis Model (PEST) (Doherty, 1994) to simultaneously analyze seven observed drawdown records from a pumping test conducted at the Cape Cod site by Moench et al. (2001). The analysis yielded comparable estimates of hydraulic conductivity (K) and specific storage (S_s) and somewhat higher values of specific yield (S_y) when compared to those obtained by Moench et al. (2001) and Tartakovsky and Neuman (2007). Their estimates of the van Genuchten–Mualem parameters were also found to be

* Corresponding author.
E-mail address: willman@uwaterloo.ca (W.A. Illman).

0022-1694/$ - see front matter Crown Copyright © 2012 Published by Elsevier B.V. All rights reserved.
http://dx.doi.org/10.1016/j.jhydrol.2012.08.044

comparable to laboratory estimates obtained for similar materials in the area. Despite the usefulness of Mishra and Neuman's (2010, 2011) solutions, they are linearized solutions that treat the medium to be homogeneous and unbounded media and thus cannot address the issue of heterogeneity, which is the rule rather than the exception.

Recently, the homogeneity assumption required by analytical solutions for heterogeneous saturated aquifers have come into question by Wu et al. (2005) and Wen et al. (2010). In particular, Wu et al. (2005) used random Gaussian fields (of transmissivity and storativity) to demonstrate that parameter estimates made using the Theis (1935) solution varied throughout the duration of the pumping test. Transmissivity estimates approached the geometric mean and storativity estimates were dominated by the material between the pumping well and the observation point. It is reasonable to expect similar limitations for analytical solutions used to estimate parameters from unconfined pumping tests. Similar results were reported by Wen et al. (2010) for field aquifer tests with a large number of observation wells.

To date, only a limited number of investigations have explicitly examined the effect of heterogeneity on pumping tests performed in unconfined aquifers (e.g., Bunn et al., 2010; Mao et al., 2011). For example, using multiple realizations of heterogeneous fields, Bunn et al. (2010) examined the connection between K heterogeneity and the capillary fringe extension phenomenon observed during a pumping test conducted by Bevan et al. (2005) at the Borden site in Canada. The ensemble mean hydraulic heads were able to reproduce the field observations quite well, however, these simulations were unable to reproduce the capillary fringe extension observed in the field data.

More recently, Mao et al. (2011) utilized the stochastic moment approach to better understand the role of heterogeneity in the development of the S-shaped drawdown curves and a cross-correlation analysis to show that drawdowns at locations in a heterogeneous unconfined aquifer are mainly affected by local heterogeneity near the pumping and observation wells. Mao et al. (2011) also critically examined the sensitivity of the S-shaped curve to the spatial variability of hydraulic parameters and concluded that it is most sensitive to hydraulic conductivity (K), specific storage (S_s) and saturated water content (θ_s) and found that it was insensitive to the variability of unsaturated hydraulic parameters.

Mapping of K heterogeneity in unconfined aquifers was recently reported by Cardiff et al. (2009) under steady-state conditions. These authors analyzed multiple drawdown data collected from fully-screened wells completed in an unconfined aquifer located at the Boise Hydrogeophysical Research Site to obtain depth-averaged K distributions through their hydraulic tomography algorithm. Various inverse methods have been developed for hydraulic tomography, which utilize pumping test data simultaneously or sequentially (e.g., Gottlieb and Dietrich, 1995; Yeh and Liu, 2000; Bohling et al., 2002; Brauchler et al., 2003, 2011; Zhu and Yeh, 2005, 2006; Li et al., 2005, 2007; Fienen et al., 2008; Castanaga and Bellin, 2009; Xiang et al., 2009; Liu and Kitanidis, 2011; Cardiff and Barrash, 2011). But to our knowledge, hydraulic tomography algorithms that can interpret the transient drawdown records from a heterogeneous, unconfined aquifer that rigorously considers the unsaturated zone does not exist except for the one developed by Zhu et al. (2011). One reason for this is that pumping in unconfined aquifers induces flow regimes in both the saturated and unsaturated zones. This demands the use of a variably saturated flow equation that considers heterogeneity for the interpretation of drawdown responses in an unconfined aquifer. Inverse modeling of flow through variably saturated and heterogeneous media is a very difficult task (Yeh and Zhang, 1996; Zhang and Yeh, 1997; Li and Yeh, 1999; Hughson and Yeh, 1998, 2000).

In this study, we investigate whether the prediction of drawdown responses in a heterogeneous unconfined aquifer and the unsaturated zone above it with a variably saturated groundwater flow model can be improved by including information on hydraulic conductivity (K) and specific storage (S_s) from transient hydraulic tomography (THT). We also investigate whether these predictions are affected by the use of unsaturated flow parameters estimated through laboratory hanging column experiments or calibration of in situ drainage curves. To investigate these issues, we designed an intermediate-scale laboratory sandbox containing a heterogeneous unconfined aquifer that was instrumented with pressure transducers, tensiometers, and water content sensors. A number of pumping tests are performed while the tank was fully saturated. These pumping tests are then used to estimate both homogeneous and heterogeneous K and S_s distributions. Parameters of the moisture release curves of different material types in the sandbox are measured using hanging water column experiments and in situ by fitting the van Genuchten (1980) model.

We next conducted another pumping test in which we allow the water table to fall, while the drawdown in the sandbox is monitored at multiple locations in the saturated zone with pressure transducers. Concurrently, we monitored the unsaturated zone with tensiometers (equipped with pressure transducers) and water content sensors. After this, we modeled the pumping test using MMOC3 (Yeh et al., 1993), a 3-D variably saturated flow and transport model to evaluate the ability of different homogeneous and heterogeneous representations of the sandbox aquifer in both the saturated and unsaturated zones to reproduce the observed drawdown responses. By comparing various idealizations of saturated and unsaturated zone parameters, we were able to find out what parameters have the greatest impacts on making accurate predictions of responses in the unsaturated and saturated zones.

2. Experimental setup

2.1. Sandbox design and instrumentation

A synthetic heterogeneous unconfined aquifer was constructed in a vertical, laboratory sandbox to investigate how the saturated and unsaturated zones respond to a pumping test that results in drainage. The sandbox was 244 cm in length, 122 cm in height, and had a thickness of 9.4 cm. A glass plate covers the front of the sandbox and a stainless steel plate covers the back. A total of one hundred four ports were drilled into the stainless plate to allow the sandbox to be instrumented with pressure transducers, tensiometers, and water content sensors.

Fifty-eight of these ports were used for the installation of fully penetrating horizontal wells (1.4 cm in diameter). In the vertical direction, these wells behave as partially penetrating wells. Each well was constructed by drilling 14 0.5-cm diameter holes along a section of brass tubing. The holes were then covered with a stainless steel mesh that was bonded to the tubing with corrosion resistant epoxy. These wells, which penetrate the thickness of the synthetic aquifer were installed after the packing of the sandbox aquifer. Additionally, 47 of these wells contain 0–2 psig pressure transducers (Model S35) from BHL Instruments. Eleven wells did not contain pressure transducers, but were still able to be used for pumping purposes.

Twenty-two of the ports (located in the upper portion of the sandbox) were used for the installation of column tensiometers (CL-029B Flow Cell Tensiometer, Soil Measurement Systems) equipped with Microswitch pressure transducers. The remaining 24 ports (also located in the upper portion of the sandbox) were instrumented with EC5 water content sensors (Decagon Devices Inc.). All sensors were connected to a National Instruments

Compaq Data Acquisition System (NIDAQ) (Model #9178) which allows for real-time monitoring of signals during pumping tests. Fig. 1 is a photograph of the sandbox showing the locations of the sensors.

For this particular study, all boundaries except the upper boundary are no-flow boundaries. The top boundary was set as a constant head boundary for the saturated pumping tests performed for characterization purposes, and left open to the atmosphere for the unconfined pumping test.

2.2. Packing of sandbox and types of sands used

Prior to the installation of the wells and tensiometers, and concurrent with the installation of the water content sensors, the sandbox was packed with commercially sieved silica sand (six types; F35, F45, F65, F75, F85, and F110) and silt (four types; Sil-co-sil 45, Sil-co-sil 53, Sil-co-sil 106, and Sil-co-sil 250) from US Silica. The grain size distributions, as reported by US Silica, for these materials used to pack the sandbox are presented in Fig. S1. This material was packed to match a heterogeneity pattern drawn on the glass side of the sandbox. The sand was slowly added to the sandbox through a tube to create thin layers (approximately 0.5–1 cm thick) and packed between each addition to achieve uniform compaction (e.g., Illman et al., 2007, 2010; Berg and Illman, 2011).

After the sand box was filled, CO_2 gas was injected into the sandbox to displace the air trapped during packing. Over a period of 3 days, CO_2 was injected at a low pressure (2–5 psi) from a number of different ports working from the bottom of the sandbox to the top. The top of the sandbox was sealed except for a small hole that allowed the gas to exit. After all of the CO_2 was pushed through the sandbox de-aired water was added at port 3 under a differential head of approximately 10–20 cm. This meant that any air above the water level would be displaced out the top of the sandbox. Since the air in the sandbox was replaced with CO_2, any trapped gas would readily dissolve into the water phase. This procedure minimized the risk of air entrapment and ensured the sandbox was fully saturated.

The predominant materials in the sandbox are the medium sands F35 and F45. Within these sands are discontinuous layers of finer grained material that average 0.8–1 m in length and average 10–15 cm thick. The most notable features of this heterogeneity pattern are the three discontinuous lenses near the top of the sandbox (Sil-co-sil 106 in the top left, Sil-co-sil 53 in the upper middle, and F110 in the top right). These lenses (in particular the silt lenses) are expected to have significantly different saturated and unsaturated properties than the surrounding F35 and F45 sand. Near the bottom of the sandbox, the most salient feature is a layer of silt (Sil-co-sil 250) that extends along the length of the sandbox expect for near the middle where a window is present. This window connects the F35 sand layer below with the F35 layer above.

Fig. 1. Photograph of the sandbox showing all sensor locations (● = pressure transducers; ● without pressure transducers; ○ = tensiometers; and **x** = water content sensors) and the various layers that were packed. Sensor locations are approximate.

3. Characterization of aquifer heterogeneity

The analysis of pumping tests performed in unconfined aquifers requires the knowledge of both saturated and unsaturated parameters. Our analysis will require the knowledge of K, S_s, θ_s (saturated moisture content), θ_r (residual moisture content), and the van Genuchten (1980) fitting parameters describing the primary drainage curve (α and n).

3.1. Characterization of K and S_s

A number of pumping tests were performed for characterization purposes while the sandbox was fully saturated. During these tests, the top boundary of the sandbox was maintained as a constant head boundary by having 3 cm of standing water in the top portion of the sandbox (above the sand). The extraction line was connected to the desired well and the pump was operated long enough to fill the effluent line (which discharged into the top reservoir, creating a loop and ensuring mass balance). Once the line was filled the pump was turned off and the system was allowed to return to equilibrium (static), before the next pumping test was started.

Sixteen ports were chosen for these pumping tests (Fig. 2). During these tests, one port was pumped, while the pressure responses within the sandbox were simultaneously monitored at 47 points sampling at a rate of 4 Hz. The pumping rates for all cross-hole tests was 240 mL/min. Prior to the pumping tests, all pressure transducers were calibrated to ensure accurate data collection. We then collected hydraulic head data for several minutes in all pressure transducers to establish a static, initial condition. After establishment of static conditions, we pumped from each port using a peristaltic pump, while taking head measurements at all 47 ports. For each test, pumping continued until the development of steady state conditions (approximately 1–2 min), which was determined by observing the stabilization of all head measurements on the data logger connected to a computer. After reaching

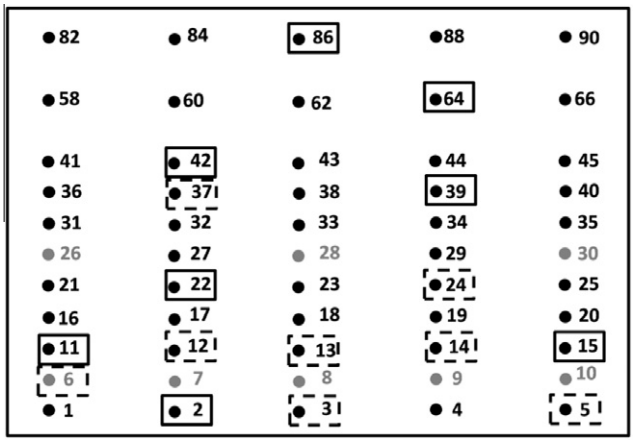

Fig. 2. Schematic diagram showing the ports that were pumped for the pumping tests. Solid black circles represent locations of pressure transducers and solid grey circles represent ports that were not instrumented. Solid squares are pumping locations used for the estimation of heterogeneous K and S_s fields. Dashed squares are pumping locations for the validation of the results from transient hydraulic tomography.

steady state, the pump was shut off and recovery data were collected.

Analysis methods for interpreting pumping test data, whether for confined, semi-confined, or unconfined aquifers often assume the aquifer to be homogeneous, however, this is rarely the case. As such, the pumping test data collected in this sandbox are analyzed in two ways; (1) a single pumping test is used to estimate effective K and S_s values (Section 3.1.1) and, (2) eight pumping tests are used to create heterogeneous K and S_s estimates using hydraulic tomography (Section 3.1.2). The remaining eight pumping tests are then used to validate these heterogeneous fields generated through hydraulic tomography.

3.1.1. Estimation of effective K and S_s

Using a pumping test performed at port 22, the parameter estimation program PEST (Doherty, 1994) was coupled with MMOC3 (Yeh et al., 1993) to estimate effective K and S_s values representing the entire domain by fitting all the drawdown curves simultaneously. The synthetic aquifer was discretized into 3645 elements and 7544 nodes with average element dimensions of 3.0 cm × 9.4 cm × 2.5 cm. The model domain was one element thick. The top boundary was set to be a constant head boundary and the remaining boundaries of the sandbox were no-flow boundaries. Six data points (at t = 1, 5, 10, 20, 40, and 80 s) from 46 ports totalling 276 data points were used for parameter estimation. The initial guesses of K and S_s were 0.1 cm/s and 1×10^{-4} cm^{-1} respectively.

The estimated effective K was 1.85×10^{-2} cm/s (with lower and upper 95% confidence bounds of 1.76×10^{-2} cm/s and 1.94×10^{-2} cm/s respectively), and the estimated effective S_s was 3.94×10^{-5} cm^{-1} (with lower and upper 95% confidence bounds of 3.40×10^{-5} cm^{-1} and 4.57×10^{-5} cm^{-1} respectively). The estimated parameters were then used to simulate the pumping test at port 22, essentially testing the calibration of the effective parameters. Fig. S2 is a calibration scatter plot (observed vs. simulated drawdown) for the pumping test at port 22. This plot shows the ability of these effective values to reproduce the observed drawdown. The dashed line represents the 1:1 line which would be a perfect match between simulated and observed. The linear model fit (solid line) has a slope near 1 suggesting that the effective values capture the average response in the sandbox for this pumping test. The scatter as indicated by the coefficient of determination (R^2) with a value of 0.80 suggests that the details of the heterogeneity are not accurately captured. This is expected since homogeneous values of K and S_s were used for this simulation.

3.1.2. Estimation of heterogeneous K and S_s

The Sequential Successive Linear Estimator (SSLE) code developed by Zhu and Yeh (2005) was used to conduct transient hydraulic tomography with multiple pumping tests performed under fully saturated conditions to obtain a heterogeneous distribution of K and S_s (from now on referred to as K and S_s tomograms). The model domain used for this inversion is identical to the one used for estimation of effective K and S_s described in Section 3.1.1.

Inputs to the inverse model include initial guesses based on available data (e.g., core data, pumping tests, etc.) for the K (0.1 cm/s) and S_s (1×10^{-4} cm^{-1}), estimates of variances ($\sigma^2_{\ln K} = 3.0$ and $\sigma^2_{\ln Ss} = 3.0$) and estimated correlation scales for both K (λ_x = 150 cm and λ_z = 20 cm) and S_s (λ_x = 150 cm and λ_z = 20 cm), volumetric discharge (Q_n) from each pumping test where n is the test number, as well as head data at various times selected from the head-time curve. We note that Yeh and Liu (2000) found that provided a large amount of hydraulic data is available (e.g., many pumping tests with a large number of observation points) as in the case with this sandbox, the initial estimates used for SSLE have a negligible effect on the resulting tomograms. Although available point (small-scale) measurements of K and S_s can be input to the inverse model, we do not use these measurements to condition the estimated parameter fields as this has the potential to introduce error if the values are not accurate (Illman et al., 2008).

In total, we utilized 8 independent tests with pumping taking place at ports 2, 11, 15, 22, 39, 42, 64 and 86 for the transient hydraulic tomography analysis. More specifically, we utilized 6 data points (at t = 1, 5, 10, 20, 40, and 80 s) from 46 ports totalling 276 data for each test. We excluded the data from the pumped port because of possible skin effects (e.g., Illman et al., 2007; Berg and Illman, 2011). In total, we utilized 2208 data points from 8 different tests in our transient inversions.

All computations for transient hydraulic tomography analyses were executed using 44 of 48 processors on a PC-cluster consisting (of 1 master and 12 slaves each with Intel Q6600 Quad Core CPU running at 2.4 GHz with 16 GB of RAM per slave) at the University of Waterloo. The operating system managing the cluster was CentOS 5.3 based on a 64-bit system. The total computational time for inverting data from 8 pumping tests was approximately 24 h. With the inclusion of each test, the parameter variance (Ln K and Ln S_s)

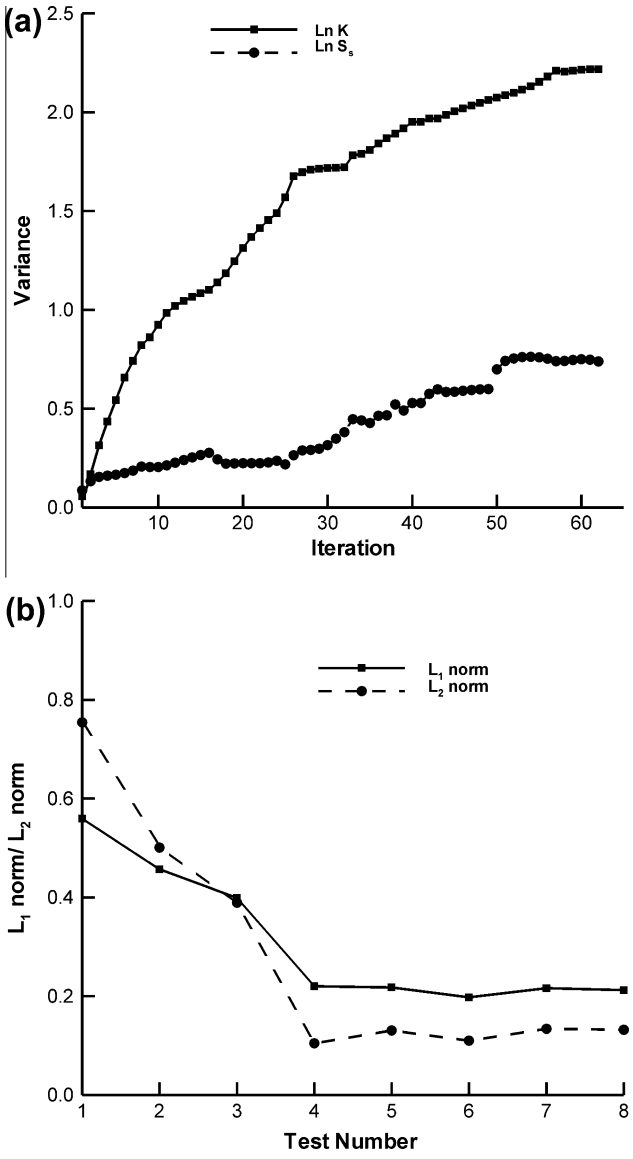

Fig. 3. (a) Ln K and Ln S_s variance versus number of iterations in the SSLE inversion (8 iterations per pumping test), and (b) L_1 and L_2 norms vs number of pumping tests included in the inversion.

and L_1 and L_2 norms (between simulated and observed drawdown) were monitored (see Fig. 3a and b respectively). Fig. 3a shows that the variance of Ln K and Ln S_s plateaus after approximately 50–60 iterations (8 iterations per tests). Additionally, Fig. 3b shows that after the 4th test, the inclusion of additional tests does not improve the L_1 and L_2 norms. As such, the inclusion of more than 8 tests for this particular sandbox is not likely to significantly improve the estimated K and S_s tomograms.

The resulting K and S_s tomograms are shown in Fig. 4a and b. A visual comparison of the K tomogram to the deposits (Fig. 1) shows that many of the important features are captured. Of particular note are the low K zones which compare very favourably with the real distribution. The two low K layers extending towards the middle from both sides near the bottom of the sandbox are present, as well as the two low K zones near the top left (there is even some indication in the tomogram that these may not be connected, which is the case). Additionally, the Sil-co-Sil 106 layer near the middle right of the sandbox is captured, however, it does not extend all the way to the boundary. This is not surprising considering there are no observation points in this region, thus, estimates here have greater uncertainty. The K tomogram also preserves the connectivity of the high K units, particularly the window in the silt (Sil-co-sil 250) layer near the bottom middle, and the large window in the silt near the top right. Thus, we feel confident that the K tomogram reflects the heterogeneity of the sandbox.

Examination of the S_s tomogram (Fig. 4b) reveals a trend of increasing S_s values with increasing elevation within the sandbox. Such a trend was also observed in the S_s values from separate sandbox studies packed using different methods, and containing different heterogeneity patterns (Liu et al., 2007; Berg and Illman, 2011). A likely explanation for this pattern being witnessed in several sandbox studies is that the material near the bottom of the sandbox is much less compressible due to the weight of the overlying material, thus, resulting in low S_s values near the bottom of the sandbox and higher S_s values near the top. Additionally some heterogeneity in the distribution of S_s is present within this trend from top to bottom, however, it does not appear to be strongly correlated with any of the features seen in the K tomogram (Fig. 4a) or the picture of the sandbox (Fig. 1). This suggests that the vertical trend in S_s is the dominant feature controlling the drawdown response in the sandbox.

The K and S_s tomograms were then rigorously tested through the simulation of pumping tests used to create the tomograms (calibration) as well as through the simulation of independent pumping tests (validation). Details of this procedure as well as scatterplots showing the performance of the tomograms (Fig. S3) are included in the Supplementary Information section. The results of this assessment indicated that the K and S_s tomograms are a reasonably accurate representation of the heterogeneous aquifer in the sandbox.

Additionally, Fig. S4 presents the variance maps of ln K and ln S_s estimates. This figure indicates that estimates of K and S_s in the central portion of the tank are estimated with reasonable accuracy; however, there is less certainty near the edges of the tank. This is particularly true for S_s and may partially explain the large range in S_s values seen the in the tomogram in Fig. 4b.

3.1.3. Estimation of θ_s, θ_r, α and n using the hanging water column method

Using the hanging water column method (Stephens, 1995), the primary drainage phase of the moisture release curve was measured for five of the materials packed in the sandbox (F35, F45, F110, Sil-co-Sil 53, and Sil-co-Sil 106). These materials were selected because they are located in the upper portion of the sandbox and are likely to experience negative pressure heads as a result of a possible release of water, when the water table is lowered during drainage or an unconfined pumping test.

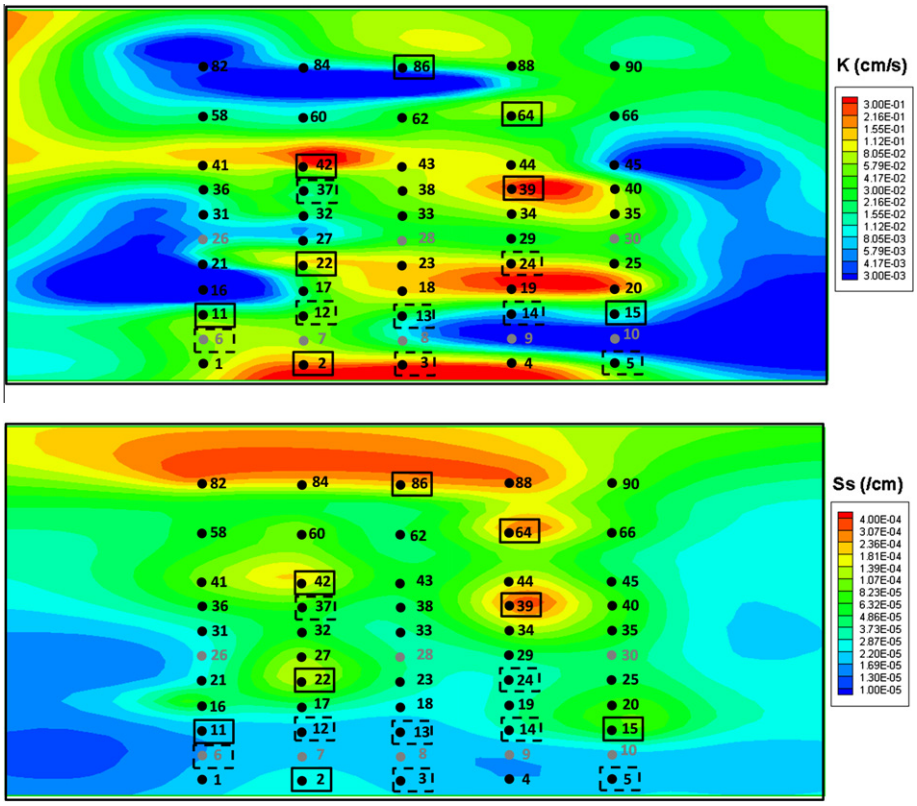

Fig. 4. (a) K and (b) S_s tomograms computed using the transient hydraulic tomography code of Zhu and Yeh (2005) with 8 pumping tests. Solid squares are pumping locations used for transient hydraulic tomography and dashed squares are pumping locations for the validation of the results.

Negative pressure head was increased incrementally until either residual water content was reached, or a value of −100 cm was achieved. A value of −100 cm was selected because it is unlikely that values greater than this will be seen during unconfined pumping or drainage tests in the sandbox. The van Genuchten (1980) model was fit to the primary drainage curves for each material by varying the α and n parameters using the Generalized Reduced Gradient (GRG2) Algorithm implemented in Excel, except for Sil-co-Sil 53 and 106 which were fit manually because the solver failed to converge for these two cases. In this analysis, the residual water content was estimated from the moisture characteristic curve and fixed during the regression. The model fit to the moisture characteristic curve, optimized parameters and the associated coefficient of determination (R^2) are presented in Fig. 5. The parameter values obtained for each of these materials (Fig. 5a–e) can be used to construct a heterogeneous case for the model domain, however, this level of detail is rarely available and a single 'effective' drainage curve would be used to describe the entire domain.

To obtain an effective α and n representing the entire aquifer domain, we fit the van Genuchten (1980) model to the primary drainage curves for both F35 and F45 simultaneously (Fig. 5f). These two sands were selected because they comprise the majority of the material in the unsaturated zone and will therefore largely control the drainage response. The other materials present in the unsaturated zone (F110, Sil-co-Sil 53, and Sil-co-Sil 106) were not included in this simultaneous match as they are only present in minor portions of the unsaturated zone and are present as discontinuous lenses. Since they are present as discontinuous lenses, it is possible that when the coarser F35 and F45 material drains, these lenses will become disconnected from the main aquifer and will not be able to effectively release their water. Thus, only the two dominant material types in the upper portion of the sandbox are selected for this effective parameter estimation.

3.1.4. Estimation of θ_s, θ_r, α and n using in situ data

Since packing can have a significant effect on the drainage behavior of soils, the values estimated using the hanging column method may not accurately reflect the unsaturated zone properties of the sands in the tank. As such, the tank was drained by pumping (explained in more detail in Section 4). While the water table was being lowered, the change in water content and the associated change in pressure head were recorded within the sandbox. Fig. 6 is a schematic diagram showing the locations of pressure transducers, tensiometers, and water content sensors installed in the sandbox as well as the port pumped for this test.

The data collected by these sensors allowed for estimation of 22 drainage curves in a manner similar to that depicted in Fig. 5. Table 1 summarizes the parameters for each of the 5 material types located in the upper portion of the sandbox. For each material type, the mean of each of the parameters in Table 1 were calculated. The number of drainage curves per material type ranged from 2 for Sil-co-sil 106 to 9 for F35 and are indicated in Table 1.

4. Unconfined pumping test

After the sandbox was characterized using pumping tests while fully saturated, the water table was allowed to fall under unconfined conditions. The objective of this test was to collect data from both the saturated and unsaturated zones during a pumping test so that we can compare the observations to variably saturated flow simulations constructed from our characterization efforts.

The pumping test started with the sandbox fully saturated and the water table at the same elevation as the top of the sand. This was confirmed visually using a manometer to get an independent reading of the static water level. Prior to the beginning of the test all sensors were monitored for several minutes to check for sensor stability and to record baseline data. This baseline data are then used as the $t = 0$ s reference to which the data collected during

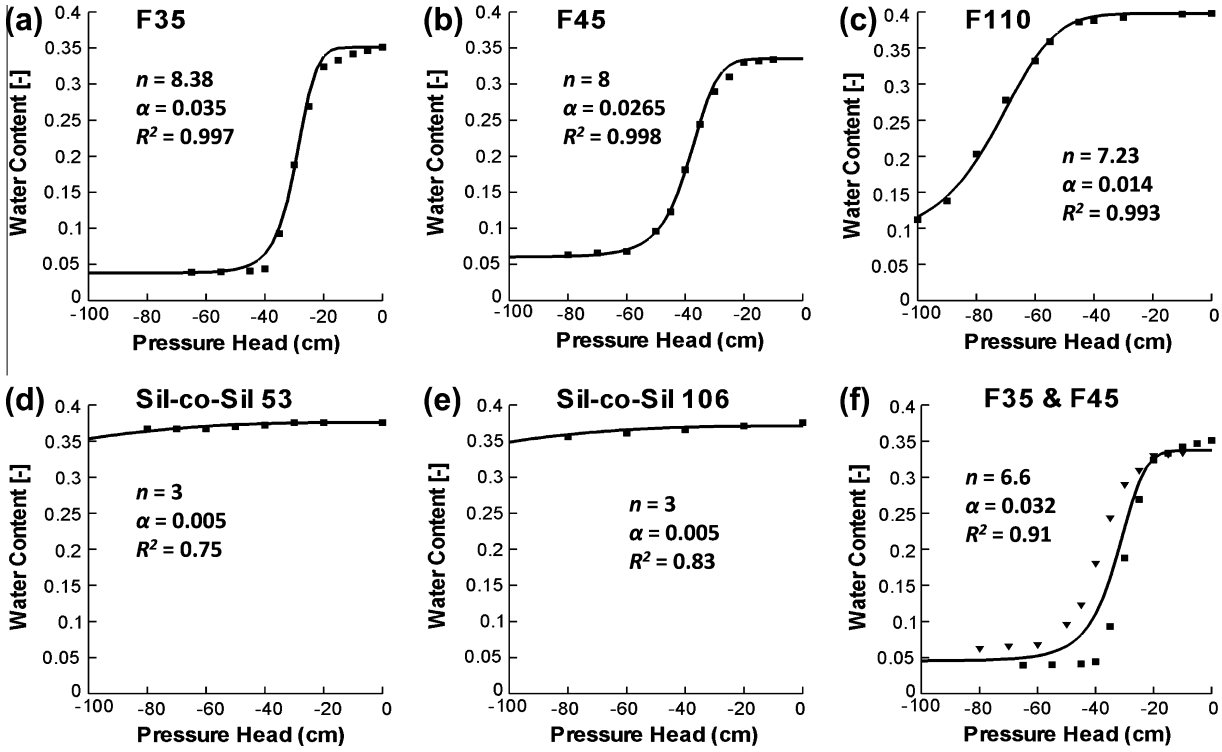

Fig. 5. Moisture characteristic curves determined through the hanging column method of: (a) F-35; (b) F-45; (c) F110; (d) Sil-co-Sil 53; (e) Sil-co-Sil 106; and (f) F35 and F45 matched simultaneously. The squares represent F35 and the inverted triangle symbols represent F45.

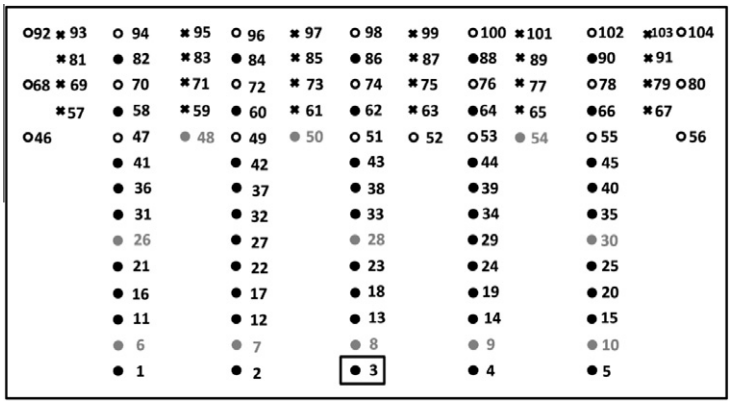

Fig. 6. Schematic diagram of the sandbox showing an array of sensors (● = pressure transducers; ● = port without pressure transducers; ○ = tensiometers; and **x** = water content sensors) utilized to monitor the pumping test in a heterogeneous unconfined aquifer. The box indicates the port at which the unconfined pumping test was performed.

Table 1
In-situ estimates of unsaturated parameters for the materials located in the upper portion of the sandbox.

Material type	θ_s	θ_r	α	N	Number of curves
F35	0.33	0.07	0.05	6.22	9
F45	0.33	0.04	0.05	6.40	5
F110	0.33	0.08	0.04	6.83	3
Sil-co-sil 106	0.37	0.07	0.06	8.25	2
Sil-co-sil 53	0.45	0.09	0.06	5.33	3

the test can be compared. Port 3 (located at the bottom middle of the sandbox) was then pumped at a rate 60 ml/min for 7.5 h. The signal from pressure transducers, tensiometers, and water content sensors was recorded for the duration of the test.

Fig. 7 shows the drawdown as measured at selected pressure transducers (Fig. 7a) and tensiometers (Fig. 7b). The ports in these figures are organized such that their positions relative to each other reflect their relative positions within the sandbox. For example, Port 58 is located left of Port 62 and above Port 31. Fig. 6 can be used as a reference to determine the absolute location of each port within the sandbox. The response measured at all ports is available online as Supplementary Fig. S5a–b.

The pressure transducers (Fig. 7a) are only able to measure the pressure response within the saturated zone. As the test progresses and the water table lowers, some of the upper wells drain, and the pressure transducer is no longer able to measure a change in pressure. The plateau in the signal for the upper ports (Ports 58, 62, and 66) in Fig. 7a reflects this process. The shape of the drawdown curves are very different from what would be expected for a fully saturated system and reflect the unconfined nature of this test. The early portion of the curves display characteristic S-shaped behavior of pumping tests performed in an unconfined aquifer. The S-shape is more pronounced for deep ports (further below the water table) than for shallow ports. This observation is consistent with that of Nwankwor et al. (1992) and Bevan et al. (2005). At late time, the observed drawdown increases again, deviating from the classical S-shaped unconfined drawdown curve. We attribute this to presence of no flow boundaries causing additional drawdown at late time. We also attribute the large early time drawdown at the pumping well (Port 3 of Fig. 7a) to possible skin effects.

The tensiometer responses measured during this test are shown in Fig. 7b. Since the water table at the start of the test was coincident with the top of the sand in the sandbox the tensiometers were initially located below the water table. By calibrating the tensiometers for this range, these tensiometers record a continuous signal as the water table drops past them (i.e. they record both positive and negative pressure head). Thus, unlike the pressure transducers installed in wells (Fig. 7a), the tensiometers are able to record a signal for the entire duration of the test. Initial inspection of Fig. 7b seems to suggest that the S-shaped curve is present in the tensiometer response. However, upon closer inspection, the S-shape at early time is missing and it is the additional late time drawdown caused by the no flow boundaries that creates the impression of an S-shape at late time. Some of the bottom tensiometers (Ports 46–52) appear to have a slight S-shape at early time, however, it is not very prominent and sensor noise makes it difficult to make any concrete statements about this. Pressure transducers at similar elevations (Fig. 7a: Ports 58–66) also do not have a very pronounced S-shape at early time. Tensiometer data collected by Nwankwor et al. (1992) during a pumping test at CFB Borden shows a very slight S-shaped response at early time only for ports near the pumping well. Thus, the absence of an S-shaped response in the tensiometer data here is not surprising. Ports 92, 98, and 104 (located in the top row of the sandbox) appear to plateau at late time. This likely indicates that the sands there are now disconnected from the main body of water, thus, the continued drop of the water table no longer influences the sands in this region.

Fig. 8 shows spatial distributions of pressure head (Fig. 8a) and water content (Fig. 8b) at $t = 400$, 2000, 8000, and 27,000 s after pumping began at port 3. The pressure and water content data were interpolated using the inverse distance weighting method. We point out that the curvature of pressure head seen along the side boundaries is an artefact of the interpolation procedure. Fig. 8a reveals that based on the pressure head distributions, an unsaturated zone begins to develop as early as $t = 400$ s. Subsequent pressure head distributions reveal that the water table drops with time and at $t = 27{,}000$ s, we notice the impact of the heterogeneity (i.e., the low K zone) on the contours of the pressure head. Based on this figure, the water table is approximately 50 cm from the bottom of the aquifer.

Fig. 8b shows the spatial distribution of the volumetric water content profiles in the upper half of the sandbox. Volumetric water content is generally uniform at the beginning of the test, but we see the impacts of pumping at $t = 8000$ s in which the water content begins to decrease near the top of the aquifer. A region of slightly higher water content is visible near the top of the aquifer indicating the presence of a low K, high porosity layer. As the pumping test continues, the pore space drains throughout the aquifer except for the low K lens which retains some of its water due to capillarity. By $t = 27{,}000$ s, the upper portion of the aquifer is at or near residual water content (shown as dark blue) although some water is still retained in the low K lens.

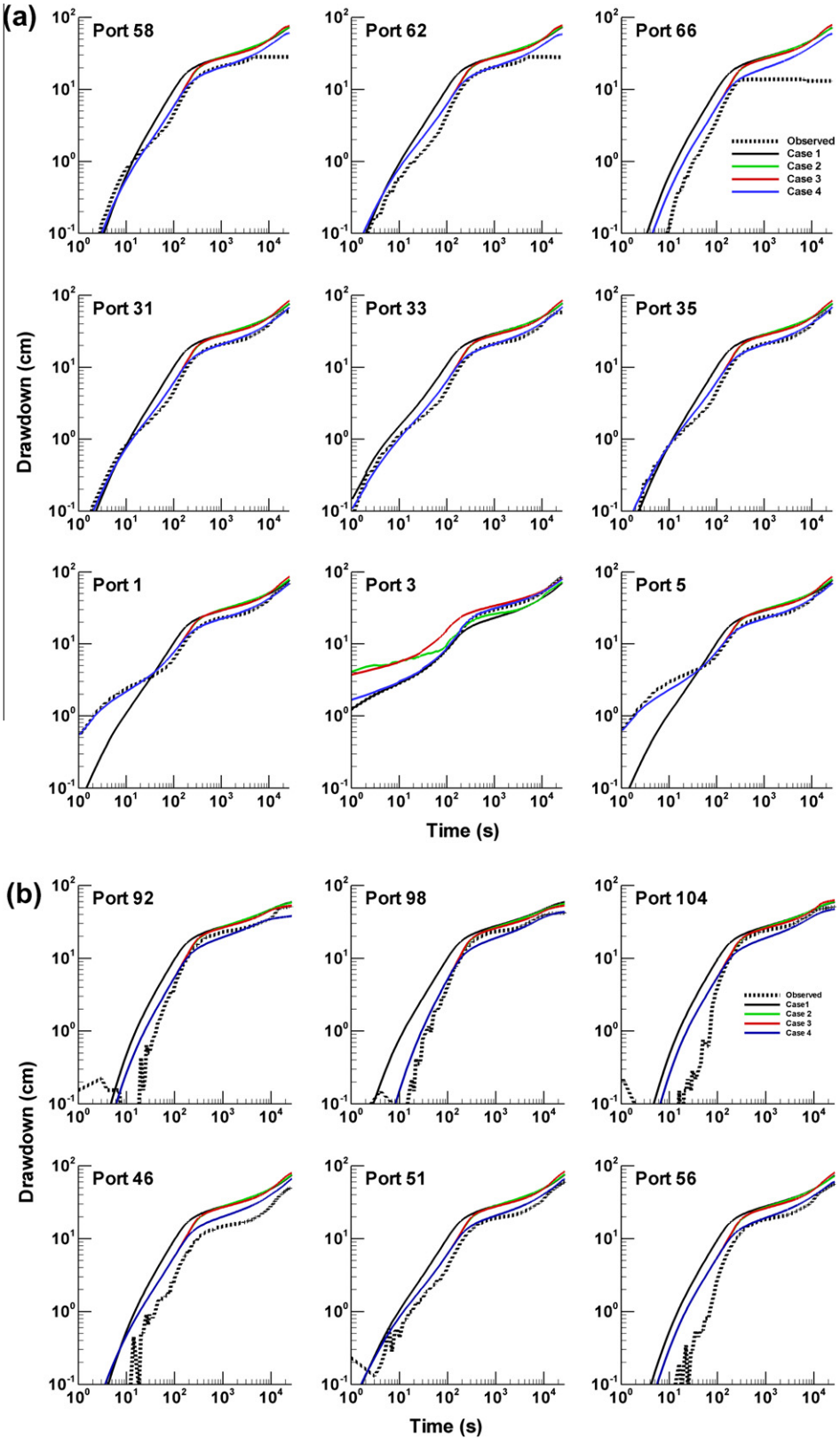

Fig. 7. Observed drawdown during the unconfined pumping test at: (a) 9 pressure transducer ports; and, (b) 6 tensiometers for the observed drawdown (dashed line), case 1 (solid black line), case 2 (green), case 3 (red), and case 4 (blue) The responses measured at all ports are available online as Supplementary Fig. S5a and b.

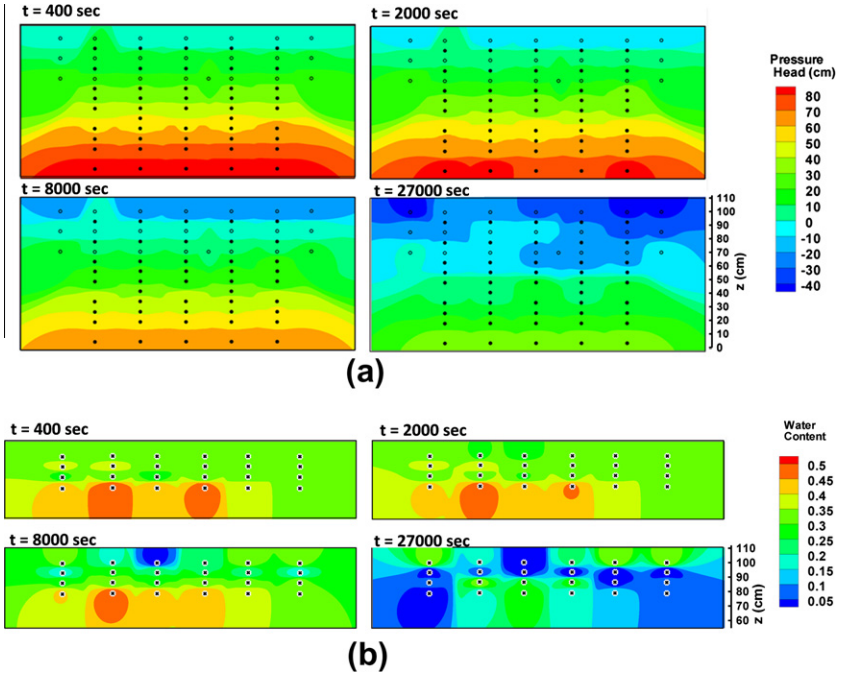

Fig. 8. Spatial distribution of: (a) pressure head and (b) volumetric water content in the upper half of the sandbox with time during the unconfined aquifer pumping test at port 3. Symbols indicate the position of various sensors used to monitor the pumping test (● = pressure transducers; ○ = tensiometers; and **x** = water content sensors).

5. Variably saturated flow modeling of pumping test in an unconfined aquifer

We next utilize the homogeneous and heterogeneous values of K, S_s, n, and α for predicting the response of the unsaturated and saturated zones during the unconfined pumping test that we described in Section 4. A finite-element numerical model, MMOC3 developed by Yeh et al. (1993) is used for these calculations. This program solves the partial differential equation that describes flow in 3-D, variably saturated geologic media:

$$\nabla \cdot [K(\psi,\mathbf{x})\nabla(\psi+z)] = \omega S_s(\mathbf{x})\frac{\partial\psi}{\partial t} + \frac{\partial\theta}{\partial t} = (\omega S_s(\mathbf{x}) + C(\psi,\mathbf{x}))\frac{\partial\psi}{\partial t} \quad (1)$$

where ∇ is the spatial gradient, $K(\psi,\mathbf{x})$ is the unsaturated hydraulic conductivity function, ψ is the pressure head where it is positive in the saturated zone, while negative in the unsaturated zone, $\mathbf{x}$ is spatial coordinates, z is the elevation, ω is the saturation index, $S_s(\psi,\mathbf{x})$ is specific storage, t is time, θ is volumetric moisture content, and $C(\psi,\mathbf{x})$ is the soil moisture capacity derived from the moisture/pressure constitutive relationship. The saturation index is equal to 1, when the porous medium is fully saturated and zero, when it is unsaturated. The program employs the Newton–Raphson iteration scheme to solve the nonlinear finite element approximation of Eq. (1).

We use MMOC3 to simulate flow to a well due to pumping in a 2-D unconfined aquifer. The dimension of the aquifer is 2.44 m × 0.094 m in the horizontal plane and 1.12 m in the vertical and is discretized into 3645 finite elements and 7544 nodes. A non-uniform mesh is used for the discretization in which some elements are larger than others so that the elements line up properly with the ports.

A no-flux boundary is assigned to the top (no infiltration or evaporation) and no-flux boundaries are imposed on the other five sides of the aquifer. The initial pressure head distribution in the aquifer is set to be hydrostatic with the water table at $z = 1.12$ m, representing a static condition. Pumping takes place at Port 3, located 7.3 cm from the bottom center of the aquifer with a constant pumping rate 60 cm^3/min. Because pumping takes place at a point, we neglected borehole storage which we consider to be a minor effect.

The hydraulic conductivity-pressure head and moisture-pressure head constitutive relationship of the aquifer are described by the model by van-Genuchten (1980):

$$\theta(\psi) = \theta_r + (\theta_s - \theta_r)(1 + \alpha|\psi|^n)^{-m} \quad (2)$$

where | | is absolute value, θ_s is the saturated moisture content, θ_r is the moisture content at residual saturation and α, n, and m are shape-fitting parameters with $m = 1-1/n$. We further assume that the $K(\Psi)$ follows Mualem's (1976) pore-size distribution model expressed as:

$$K(\psi) = K_s\frac{\{1-(\alpha|\psi|)^{n-1}[1+(\alpha|\psi|)^n]^{-m}\}^2}{[1+(\alpha|\psi|)^n]^{m/2}} \quad (3)$$

where K_s is the locally isotropic saturated hydraulic conductivity; and α, n, and m are the same as those in Eq. (2). The K_s and S_s were estimated earlier from the pumping tests described in Section 3.1., while the unsaturated zone parameters for the van Genuchten–Mualem model were obtained through the hanging water column (3.1.3) or through the calibration of in situ drainage curves (3.1.4).

5.1. Case 1: Homogeneous saturated and unsaturated zone parameters

In case 1, we obtained effective K and S_s estimates for the pumping test performed at Port 22 by coupling MMOC3 with the parameter estimation PEST. The resulting PEST estimated K and S_s values were 1.85×10^{-2} cm/s and 3.94×10^{-5} cm^{-1} respectively. We also used the van-Genuchten model parameters ($\alpha = 0.032$ and $n = 6.6$) estimated from a simultaneous match of drainage curves from the hanging column method for sands F35 and F45 (Fig. 5f) to obtain a homogeneous estimate for the unsaturated zone parameters.

Forward simulation results for the pumping test under unconfined conditions are shown in Fig. 7. In particular, Fig. 7a shows the simulated (solid black line) versus the observed (dashed line) drawdowns from selected pressure transducers in the saturated

zone, while Fig. 7b shows a similar comparison for pressure transducers installed in the unsaturated zone. Fig. 7a and b reveals that the comparison between the simulated and observed drawdowns in both the saturated (Fig. 7a) and unsaturated (Fig. 7b) zones is poor. The simulated drawdown is generally greater than the observed, especially at intermediate and late time. Early time drawdown at pressure transducers are overestimated at some ports and underestimated at others. This is attributed to the homogeneous K and S_s fields which, captures the heterogeneity in an average sense, and thus, is not expected to accurately simulate the response at all ports. Supplementary Fig. S5 shows the observed and simulated drawdown response for all pressure transducers and tensiometers.

5.2. Case 2: Heterogeneous saturated parameters and homogeneous unsaturated zone parameters

In case 2, we obtained the K and S_s fields through transient hydraulic tomography of 8 separate pumping tests. The treatment of unsaturated zone parameters is identical to case 1 (effective homogeneous values). Forward simulation results (solid green line) shown in Fig. 7a for the saturated zone reveals a marked improvement in the prediction of drawdowns for early to intermediate times, while drawdowns are overestimated at late times. On the other hand, we observe that the drawdown predictions in the unsaturated zone (Fig. 7b) are slightly improved, but still not very good showing that the simulated values generally exceeding the observed values especially at early time. This discrepancy could be attributed to a number of factors such as heterogeneity in unsaturated zone parameters and also due to a delay in response of the tensiometers. Supplementary Fig. S5 shows the observed and simulated drawdown response for case 2 for all pressure transducers and tensiometers.

5.3. Case 3: Heterogeneous saturated parameters and heterogeneous unsaturated zone parameters

To investigate the cause of discrepancy of drawdowns observed in the unsaturated zone, we also considered in case 3 (solid red line), the variability of the unsaturated zone parameters by assigning homogeneous values for each layer. In the field, information on stratigraphy may be obtained from outcrops, borehole logs, or geophysical surveys. However, the connectivity of such layers is uncertain from limited field data. In contrast, the connectivity of layers can be ascertained as the heterogeneity pattern can be verified through the glass of the sandbox. As such, having the knowledge of heterogeneity pattern provides a better experimental control for examining the impact of layering/heterogeneity of unsaturated zone parameters on drawdown responses of flow to a well in a heterogeneous unconfined aquifer. Fig. 7a reveals that the quality of matches between cases 2 and 3 are virtually identical, perhaps suggesting that heterogeneity in unsaturated zone parameters may not be that critical in responses in the saturated zone. This observation is in agreement with the findings from a numerical study conducted by Mao et al. (2011). Predictions of drawdowns in the unsaturated zone show only a slight improvement, suggesting that as long as the K and S_s are accurately known and the unsaturated parameters are represented accurately (in an effective sense), it is possible to predict unconfined pumping tests using a variably saturated flow model. Supplementary Fig. S5 shows the observed and simulated drawdown response for case 3 for all pressure transducers and tensiometers.

5.4. Case 4: Heterogeneous saturated parameters and heterogeneous unsaturated zone parameters (measured in situ)

Case 4 (solid blue line) is similar to case 3, except where case 3 uses unsaturated parameters obtained through the hanging column method (Fig. 5), while case 4 uses the values measured in situ during the drainage test (Table 1). Fig. 7a and b shows improved matches for pressure transducers and tensiometers, respectively. This improved match is especially pronounced at late time, suggesting that the ex-situ lab measured values do not match the behavior of the soil when packed in the sandbox. This is not a surprising finding as the conditions of the hanging columns experiments are different than those of the sandbox. Supplementary Fig. S5 shows the observed and simulated drawdown response for case 4 for all pressure transducers and tensiometers.

5.5. Comparison of observed versus simulated water content distributions and water table positions

Finally, we visually compared the observed (Fig. 8b) versus simulated water content distributions (Fig. 9a–d) in a bulk sense and the water table positions for the four cases examined at t = 27,000 s. We note that this comparison is qualitative in nature because the observed water content distribution is interpolated using a limited number of data. In any case, Fig. 9a (case 1) shows that the water content in the unsaturated zone is lower than the observed distribution (Fig. 8b at t = 27,000 s). We attribute this to the fact that the model for case 1 does not consider the variability in saturated and unsaturated zone parameters which allows for the drainage of water when the water table is lowered. Fig. 9b shows the results from case 2 in which heterogeneity in K and S_s is considered. This case reveals that an increased amount of water is stored in the unsaturated zone (Fig. 9b) in comparison to case 1 despite the fact that the unsaturated zone parameters are treated to be uniform, but the amount is still qualitatively less than those observed (Fig. 8b at t = 27,000 s).

In contrast, consideration of variability in the unsaturated zone parameters has a pronounced impact on the water content distributions. For example, Fig. 9c plots the water content distributions from case 3 showing that a significant amount of water is stored in the unsaturated zone, in particular, in the layers containing Sil-co-sil 106, Sil-co-sil 53, and F110 (Fig. 1). However, the amount of water stored in these layers (Fig. 9c) appears to be higher than in the observed distribution (Fig. 8b at t = 27,000 s).

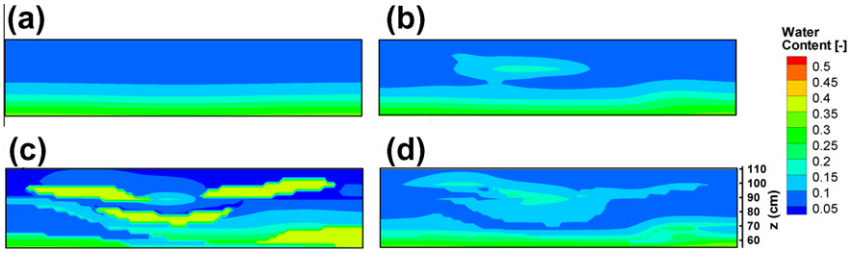

Fig. 9. Simulated water content distributions in the unsaturated zone for: (a) case 1, (b) case 2, (c) case 3, and (d) case 4 at t = 27,000 s.

Water content distributions from case 4 are next plotted in Fig. 9d. We note that the use of in situ estimates of unsaturated zone parameters results in a water content distribution that is more similar in a bulk sense to the observed distribution (Fig. 8b). This suggests that case 4, while far from perfect, when compared to cases 1–3, yields the best results in terms of reproducing the bulk water content in the unsaturated zone at late times (t = 27,000 s) after the water table has been lowered.

Additional evidence that suggests that case 4 yielded the best predictive ability in terms of the hydraulic behavior for both the saturated and unsaturated zones comes from the prediction of the approximate water table position (z) ($z \approx 43$ cm) measured from the bottom of the sandbox at t = 27,000 s, when the actual pumping test yielded $\sim$ 50 cm. This result is a significant improvement when compared to case 1 ($z \approx 35$ cm), case 2 ($z \approx 35$ cm), and case 3 ($z \approx 28$ cm). Here, the water table position is reported only as an approximate value because the heterogeneity in saturated and unsaturated zone parameters causes subtle fluctuations in the water table position. Additionally, small differences in the unsaturated zone parameters could be responsible for the error between the simulated and observed water table elevations.

6. Discussion and summary

Flow to wells due to the pumping of unconfined aquifers has been a topic of great interest for many decades. We studied the impact of the unsaturated zone and effects of heterogeneity on flow to a pumping well in an unconfined aquifer using a synthetic heterogeneous aquifer packed in an intermediate-scale laboratory sandbox. The synthetic aquifer was characterized initially with eight pumping tests under fully saturated conditions and the hydraulic data were interpreted using the transient hydraulic tomography (THT) code developed by Zhu and Yeh (2005). The resulting hydraulic conductivity (K) and specific storage (S_s) tomograms were validated using eight additional tests not used in the inverse modeling. Effective parameters of K and S_s were also estimated through the inverse modeling of an individual pumping test. Unsaturated zone parameters were determined using the hanging column method and in situ by fitting the van Genuchten (1980) model to the main drainage curves for each sand type. We then conducted another pumping test in which a port near the bottom of the aquifer was pumped at a constant rate. During this test, the water table was allowed to freely move downwards in response to pumping. The saturated zone was monitored via pressure transducers and the unsaturated zone with tensiometers and water content sensors.

Forward models of various complexities in saturated and unsaturated parameters were then built using the variably saturated code, MMOC3 (Yeh et al., 1993) to examine the sensitivity of the homogeneous and heterogeneous parameter estimates on the predictability of the unconfined aquifer test. Results show that effective K and S_s values determined through the inverse modeling of a pumping test cannot yield accurate predictions of drawdown responses in the saturated and unsaturated zones. Our predictions of drawdown responses in the saturated zone improved when the K and S_s distributions from THT were utilized in the forward simulation of the unconfined aquifer pumping test. Because we monitored the pressure changes in the unsaturated zone during this experiment, we also attempted to evaluate the predictions of pressure and water content responses in the unsaturated zone. Results showed that only slightly improved predictions of drawdowns in the unsaturated zone could be achieved if heterogeneous zones were assigned to the model. However, our results showed that predictions of drawdowns in the saturated zone were relatively insensitive to whether we conceptualized the unsaturated zone to be homogeneous or heterogeneous which confirms a conclusion reached by Mao et al. (2011) using numerical first-order uncertainty analysis.

We also found that improved predictions of drawdowns in both the saturated and unsaturated zones can be obtained when the unsaturated flow parameters determined within the sandbox were used (case 4) instead of those obtained from the hanging column method (case 3) which is done ex situ of the sandbox aquifer. This pattern of improvement was also observed for the water content distributions, with case 4 producing the most realistic water content distribution and water table position within the sandbox at 27,000 s after the start of pumping.

Based on this study, we conclude that it is possible to accurately predict the response of a heterogeneous unconfined aquifer to pumping as long as the saturated parameters (K and S_s) are accurately characterized and an accurate effective value of the unsaturated parameters is known. This study was unique in that the heterogeneity pattern was exactly known and it was possible to select effective unsaturated parameters by assessing which material would dominate the drainage response. In the field however, this is not as straightforward and the selection of unsaturated parameters could pose a challenge. Our results also showed that the prediction of water content distributions improved as more information was made available for the unsaturated zone. While these results are encouraging, we also acknowledge that these comparisons could be improved. As such, interpreting pumping tests in heterogeneous aquifers will benefit from inverse modeling of both the unsaturated and saturated zones. This will require the use of a variably saturated model coupled with an inverse algorithm such as the Sequential Successive Linear Estimator (e.g., Hughson and Yeh, 2000) for the proper interpretation of flow to wells in a heterogeneous unconfined aquifer.

Acknowledgments

This research was supported in part by Project ER-1365 through the Strategic Environmental Research and Development Program, Canada Foundation for Innovation, and Ontario Research Funds. S. Berg was also supported by the Ontario Graduate Scholarship. We thank the assistance of Andrew Price who helped conduct the laboratory experiments for his undergraduate work term at the University of Waterloo.

Appendix A. Supplementary material

Supplementary data associated with this article can be found, in the online version, at http://dx.doi.org/10.1016/j.jhydrol.2012.08.044.

References

Berg, S.J., Illman, W.A., 2011. Capturing heterogeneity in groundwater flow parameters: comparison of approaches through controlled sandbox experiments. Water Resour. Res. 47, W09514. http://dx.doi.org/10.1029/2011WR010429.

Bevan, M.J., Endres, A.L., Rudolph, D.L., Parkin, G., 2005. A field scale study of pumping-induced drainage and recovery in an unconfined aquifer. J. Hydrol. 315, 52–70. http://dx.doi.org/10.1016/j.jhydrol.2005.04.006.

Bohling, G.C., Zhan, X., Butler Jr., J.J., Zheng, L., 2002. Steady shape analysis of tomographic pumping tests for characterization of aquifer heterogeneities. Water Resour. Res. 38 (12), 1324. http://dx.doi.org/10.1029/2001WR001176.

Boulton, N.S., 1954. Unsteady radial flow to a pumped well allowing for delayed yield from storage. Publ. Int. Assoc. Sci. Hydrol., Rome. vol. 37, pp. 472–477.

Boulton, N.S., 1963. Analysis of data from non-equilibrium pumping tests allowing for delayed yield from storage. Proc. Inst. Civ. Eng. 26, 469–482.

Brauchler, R., Liedl, R., Dietrich, P., 2003. A travel time based hydraulic tomographic approach. Water Resour. Res. 39 (12), 1370. http://dx.doi.org/10.1029/2003WR002262.

Brauchler, R., Hu, R., Dietrich, P., Sauter, M., 2011. A field assessment of high-resolution aquifer characterization based on hydraulic travel time and

hydraulic attenuation tomography. Water Resour. Res. 47, W03503. http://dx.doi.org/10.1029/2010WR009635.
Bunn, M.I., Jones, J.P., Endres, A.L., Rudolph, D.L., 2010. Effects of hydraulic conductivity heterogeneity on vadose zone response to pumping in an unconfined aquifer. J. Hydrol. 387, 90–104.
Cardiff, M., Barrash, W., Kitanidis, P.K., Malama, B., Revil, A., Straface, S., Rizzo, E., 2009. A potential-based inversion of unconfined steady-state hydraulic tomography. Ground Water 47 (2), 259–270.
Cardiff, M., Barrash, W., 2011. 3-D transient hydraulic tomography in unconfined aquifers with fast drainage response. Water Resour. Res. 47, W12518. http://dx.doi.org/10.1029/2010WR010367.
Castanaga, M., Bellin, A., 2009. A Bayesian approach for inversion of hydraulic tomographic data. Water Resour. Res. 45, W04410. http://dx.doi.org/10.1029/2008WR007078.
Dagan, G., 1967. A method of determining the permeability and effective porosity of unconfined anisotropic aquifers. Water Resour. Res. 3, 1059–1071. http://dx.doi.org/10.1029/WR003i004p01059.
Doherty, J., 1994. PEST: Model-Independent Parameter Estimation. Watermark Comput., Corinda, Qld., Australia, p. 122.
Fienen, M.N., Clemo, T., Kitanidis, P.K., 2008. An interactive bayesian geostatistical inverse protocol for hydraulic tomography. Water Resour. Res. 44, W00B01. http://dx.doi.org/10.1029/2007WR006730.
Gottlieb, J., Dietrich, P., 1995. Identification of the permeability distribution in soil by hydraulic tomography. Inverse Probl. 11, 353–360.
Hughson, D.L., Yeh, T.-C.J., 1998. A geostatistically based inverse model for three-dimensional variably saturated flow. Stochastic Hydrol. Hydraul. 12, 285–298.
Hughson, D., Yeh, T.-C.J., 2000. An inverse model for three-dimensional flow in variably saturated porous media. Water Resour. Res. 36 (4), 829–839.
Illman, W.A., Liu, X., Craig, A., 2007. Steady-state hydraulic tomography in a laboratory aquifer with deterministic heterogeneity: multi-method and multiscale validation of hydraulic conductivity tomograms. J. Hydrol. 341 (3–4), 222–234.
Illman, W.A., Craig, A.J., Liu, X., 2008. Practical issues in imaging hydraulic conductivity through hydraulic tomography. Ground Water 46 (1), 120–132.
Illman, W.A., Zhu, J., Craig, A.J., Yin, D., 2010. Comparison of aquifer characterization approaches through steady state groundwater model validation: a controlled laboratory sandbox study. Water Resour. Res. 46, W04502. http://dx.doi.org/10.1029/2009WR007745.
Kroszynski, U.I., Dagan, G., 1975. Well pumping in unconfined aquifers: the influence of the unsaturated zone. Water Resour. Res. 11, 479–490. http://dx.doi.org/10.1029/WR011i003p00479.
Li, B., Yeh, T.-C.J., 1999. Cokriging estimation of the conductivity field under variably saturated flow conditions. Water Resour. Res. 35 (12), 3663–3674.
Li, W., Englert, A., Cirpka, O.A., Vanderborght, J., Vereecken, H., 2007. Two dimensional characterization of hydraulic heterogeneity by multiple pumping tests. Water Resour. Res. 43, W04433. http://dx.doi.org/10.1029/2006WR005333.
Li, W., Nowak, W., Cirpka, O.A., 2005. Geostatistical inverse modeling of transient pumping tests using temporal moments of drawdown. Water Resour. Res. 41, W08403. http://dx.doi.org/10.1029/2004WR003874.
Liu, X., Illman, W.A., Craig, A.J., Zhu, J., Yeh, T.-C.J., 2007. Laboratory sandbox validation of transient hydraulic tomography. Water Resour. Res. 43, W05404. http://dx.doi.org/10.1029/2006WR005144.
Liu, X., Kitanidis, P.K., 2011. Large-scale inverse modeling with an application in hydraulic tomography. Water Resour. Res. 47, W02501. http://dx.doi.org/10.1029/2010WR009144.
Mao, D., Wan, L., Yeh, T.-C.J., Lee, C.-H., Hsu, K.-C., Wen, J.-C., Lu, W., 2011. A revisit of drawdown behaviour during pumping in unconfined aquifers. Water Resour. Res. 47, W05502. http://dx.doi.org/10.1029/2010WR009326.
Mathias, S.A., Butler, A.P., 2006. Linearized Richards' equation approach to pumping test analysis in compressible aquifers. Water Resour. Res. 42, W06408. http://dx.doi.org/10.1029/2005WR004680.
Mishra, P.K., Neuman, S.P., 2010. Improved forward and inverse analyses of saturated-unsaturated flow toward a well in a compressible unconfined aquifer. Water Resour. Res. 46, W07508. http://dx.doi.org/10.1029/2009WR008899.
Mishra, P.K., Neuman, S.P., 2011. Saturated-unsaturated flow to a well with storage in a compressible unconfined aquifer. Water Resour. Res. 47, W05553. http://dx.doi.org/10.1029/2010WR010177.
Moench, A.F., 1997. Flow to a well of finite diameter in a homogeneous, anisotropic water table aquifer. Water Resour Res. 33, 1397–1407. http://dx.doi.org/10.1029/97WR00651.
Moench, A.F., Garabedian, S.P., LeBlanc, D.R., 2001. Estimation of Hydraulic Parameters from An Unconfined Aquifer Test Conducted in a Glacial Outwash Deposit, Cape Cod, Massachusetts. US Geological Survey Professional Paper, 1629, p. 69.
Mualem, Y., 1976. A new model for predicting hydraulic conductivity of unsaturated porous media. Water Resour. Res. 12, 513–522. http://dx.doi.org/10.1029/WR012i003p00513.
Neuman, S.P., 1972. Theory of flow in unconfined aquifers considering delayed response of the water table. Water Resour. Res. 8, 1031–1045. http://dx.doi.org/10.1029/WR008i004p01031.
Neuman, S.P., 1974. Effects of partial penetration on flow in unconfined aquifers considering delayed aquifer response. Water Resour. Res. 10, 303–312. http://dx.doi.org/10.1029/WR010i002p00303.
Nwankwor, G.I., Gillham, R.W., van der Kamp, G., Akindunni, F.F., 1992. Unsaturated and saturated flow in response to pumping of an unconfined aquifer: field evidence of delayed drainage. Ground Water 30 (5), 690–700.
Stephens, D.B., 1995. Vadose Zone Hydrology. CRC Press, Boca Raton, Florida.
Streltsova, T., 1973. Flow near a pumped well in an unconfined aquifer under nonsteady conditions. Water Resour. Res. 9 (1), 227–235.
Tartakovsky, G.D., Neuman, S.P., 2007. Three-dimensional saturated-unsaturated flow with axial symmetry to a partially penetrating well in a compressible unconfined aquifer. Water Resour. Res. 43, W01410. http://dx.doi.org/10.1029/2006WR005153.
van Genuchten, M.T., 1980. A closed-form equation for predicting the hydraulic conductivity of unsaturated soils. Soil Sci. Soc. Am. J. 44, 892–898.
Wen, J.-C., Wu, C.-M., Yeh, T.-C.J., et al., 2010. Estimation of effective aquifer hydraulic properties from an aquifer test with multi-well observations (Taiwan). Hydrogeol. J. 18 (5), 1143–1155.
Wu, C.-M., Yeh, T.-C.J., Zhu, J., Lee, T.H., Hsu, N.-S., Chen, C.-H., Sancho, A.F., 2005. Traditional analysis of aquifer tests: comparing apples to oranges? Water Resour. Res. 41, W09402. http://dx.doi.org/10.1029/2004WR003717.
Xiang, J., Yeh, T.-C.J., Lee, C.-H., Hsu, K.-C., Wen, J.-C., 2009. A simultaneous successive linear estimator and a guide for hydraulic tomography analysis. Water Resour. Res. 45, W02432. http://dx.doi.org/10.1029/2008WR007180.
Yeh, T.-C.J., Liu, S., 2000. Hydraulic tomography: development of a new aquifer test method. Water Resour. Res. 36 (8), 2095–2105.
Yeh, T.-C.J., Srivastava, R., Guzman, A., Harter, T., 1993. A numerical model for water flow and chemical transport in variably saturated porous media. Ground Water 31, 634–644.
Yeh, T.-C.J., Zhang, J., 1996. A geostatistical inverse method for variably saturated flow in the vadose zone. Water Resour. Res. 32 (9), 2757–2766.
Zhang, J., Yeh, T.-C.J., 1997. An iterative geostatistical inverse method for steady flow in the vadose zone. Water Resour. Res. 33 (1), 63–71.
Zhu, J., Yeh, T.-C.J., 2005. Characterization of aquifer heterogeneity using transient hydraulic tomography. Water Resour. Res. 41, W07028. http://dx.doi.org/10.1029/2004WR 003790.
Zhu, J., Yeh, T.-C.J., 2006. Analysis of hydraulic tomography using temporal moments of drawdown-recovery data. Water Resour. Res. 42, W02403. http://dx.doi.org/10.1029/ 2005WR004309.
Zhu, J., Yeh, T.-C.J., Mao, D., 2011. Hydraulic tomography to characterize heterogeneity of unconfined aquifers. J. Nanjing Univ., Nat. Sci. 47 (3).